Achromatic Savart polariscope: choice of materials

Tingkui Mu,[1,*] Chunmin Zhang,[1,2] Qiwei Li,[1] Lin Zhang,[1] Yutong Wei,[1] and Qingying Chen[1]

[1]*Ministry of Education Key Laboratory for Nonequilibrium Synthesis and Modulation of Condensed Matter, School of Science, Xi'an Jiaotong University, Xi'an 710049, China*

[2]*zcm@mail.xjtu.edu.cn*

[*]*tkmu@mail.xjtu.edu.cn*

Abstract: This paper presents the achromatization of Savart Polariscope to decrease the lateral-shear dispersion in the lateral displacement. The achromatic Savart Polariscope can be made from two different birefringent crystal materials. The achromatic model for the choices of material is presented. The achievements and performances of different achromatic Savart Polariscopes are demonstrated with numerical simulations and ray tracing program. The chromatic variation in lateral displacement can be reduced by an order of magnitude across the spectral range 0.4μm to 0.9μm.

OCIS codes: (230.5440) Polarization-selective devices; (220.2740) Geometric optical design; (260.1440) Birefringence; (260.1180) Crystal optics; (260.2030) Dispersion.

References and links

1. J. Courtial, B. A. Patterson, W. Hirst, A. R. Harvey, A. J. Duncan, W. Sibbett, and M. J. Padgett, "Static Fourier-transform ultraviolet spectrometer for gas detection," Appl. Opt. **36**(13), 2813–2817 (1997).
2. C. Zhang, B. Xiangli, B. Zhao, and X. Yuan, "A static polarization imaging spectrometer based on a Savart polariscope," Opt. Commun. **203**(1-2), 21–26 (2002).
3. A. R. Harvey and D. W. Fletcher-Holmes, "Birefringent Fourier-transform imaging spectrometer," Opt. Express **12**(22), 5368–5374 (2004), http://www.opticsinfobase.org/oe/abstract.cfm?uri=oe-12-22-5368.
4. T. Mu, C. Zhang, and B. Zhao, "Principle and analysis of a polarization imaging spectrometer," Appl. Opt. **48**(12), 2333–2339 (2009).
5. T. Mu, C. Zhang, W. Ren, and X. Jian, "Static dual-channel polarization imaging spectrometer for simultaneous acquisition of inphase and antiphase interference images," Meas. Sci. Technol. **22**(10), 105302 (2011).
6. A. Gorman, D. W. Fletcher-Holmes, and A. R. Harvey, "Generalization of the Lyot filter and its application to snapshot spectral imaging," Opt. Express **18**(6), 5602–5608 (2010), http://www.opticsinfobase.org/oe/abstract.cfm?uri=oe-18-6-5602.
7. J. Masiero, K. Hodapp, D. Harrington, and H. Lin, "Commissioning of the Dual-Beam Imaging Polarimeter for the University of Hawaii 88 inch Telescope," Publ. Astron. Soc. Pac. **119**(860), 1126–1132 (2007).
8. K. Fujita, Y. Itoh, and T. Mukai, "Development of simultaneous imaging polarimeter for asteroids," Adv. Space Res. **43**(2), 325–327 (2009).
9. J. D. Perreault, "Triple Wollaston-prism complete-Stokes imaging polarimeter," Opt. Lett. **38**(19), 3874–3877 (2013).
10. J. Craven-Jones, M. W. Kudenov, M. G. Stapelbroek, and E. L. Dereniak, "Infrared hyperspectral imaging polarimeter using birefringent prisms," Appl. Opt. **50**(8), 1170–1185 (2011).
11. T. Mu and C. Zhang, "Models for polarization detection with the modified polarization interference imaging spectrometer," Optik (Stuttg.) **124**(7), 661–665 (2013).
12. T. Mu, C. Zhang, C. Jia, and W. Ren, "Static hyperspectral imaging polarimeter for full linear Stokes parameters," Opt. Express **20**(16), 18194–18201 (2012), http://www.opticsinfobase.org/oe/abstract.cfm?uri=oe-20-16-18194.
13. T. Mu, C. Zhang, W. Ren, and C. Jia, "Static polarization-difference interference imaging spectrometer," Opt. Lett. **37**(17), 3507–3509 (2012).
14. T. Mu and C. Zhang, "A novel polarization interferometer for measuring upper atmospheric winds," Chin. Phys. B **19**(6), 060702 (2010).
15. N. Murakami and N. Baba, "Common-path lateral-shearing nulling interferometry with a Savart plate for exoplanet detection," Opt. Lett. **35**(18), 3003–3005 (2010).
16. S.-T. Lin, S.-L. Yeh, and M.-H. Hxieh, "Broadband light source shearing interferometer using Savart plate and angular scanning technique," Opt. Lett. **37**(11), 1907–1909 (2012).
17. C. Zhang and X. Jian, "Wide-spectrum reconstruction method for a birefringence interference imaging spectrometer," Opt. Lett. **35**(3), 366–368 (2010).

#202883 - $15.00 USD Received 10 Dec 2013; revised 27 Jan 2014; accepted 15 Feb 2014; published 25 Feb 2014

18. W. Ren, C. Zhang, T. Mu, and H. Dai, "Spectrum reconstruction based on the constrained optimal linear inverse methods," Opt. Lett. **37**(13), 2580–2582 (2012).
19. W. Ren, C. Zhang, C. Jia, T. Mu, Q. Li, and L. Zhang, "Precise spectrum reconstruction of the Fourier transforms imaging spectrometer based on polarization beam splitters," Opt. Lett. **38**(8), 1295–1297 (2013).
20. C. Zhang, W. Ren, T. Mu, L. Fu, and C. Jia, "Empirical mode decomposition based background removal and de-noising in polarization interference imaging spectrometer," Opt. Express **21**(3), 2592–2605 (2013), http://www.opticsinfobase.org/abstract.cfm?uri=oe-21-8-10207.
21. N. Ebizuka, H. Yokota, F. Kajino, K. S. Kawabata, M. Iye, and S. Sato, "Novel Direct Vision Prism and Wollaston Prism Assembly for Diffraction Limit Applications," Proc. SPIE **7018**, 70184S (2008).
22. G. Wong, R. Pilkington, and A. R. Harvey, "Achromatization of Wollaston polarizing beam splitters," Opt. Lett. **36**(8), 1332–1334 (2011).
23. P. Hariharan, "Archromatic retarders using quartz and mica," Meas. Sci. Technol. **6**(7), 1078–1079 (1995).
24. J. Liu, Y. Cai, H. Chen, X. Zeng, D. Zou, and S. Xu, "Design for the optical retardation in broadband zero-order half-wave plates," Opt. Express **19**(9), 8557–8564 (2011), http://www.opticsinfobase.org/oe/abstract.cfm?uri=oe-19-9-8557.
25. J. Craven-Jones, M. W. Kudenov, M. G. Stapelbroek, and E. L. Dereniak, "Infrared hyperspectral imaging polarimeter using birefringent prisms," Appl. Opt. **50**(8), 1170–1185 (2011).
26. M. Françon and S. Mallick, *Polarization Interferometers: Applications in Microscopy and Macroscopy* (Wiley-Interscience, New York, 1971), pp. 19–25, 141–145.
27. W. J. Tropf, M. E. Thomas, and E. W. Rogala, "Properties of Crystals and Glasses," in Chapter 2 in Vol. 4 of *Handbook of Optics*, 3 ed., M. Bass, ed. (McGraw-Hill, New York, 2010), pp. 2.60–66.
28. L. L. C. Radiant Zemax, *http://www.zemax.com/*.

1. Introduction

Polarizing beam splitters, Savart polariscope (SP) and Wollaston prism (WP), are proving to be very popular in a number of occasions of being used such as spectrometry [1–6], polarimetry [7–9], spectropolarimetry [10–13], and interferometry [14–16], etc.. Since SP and WP are usually made of birefringent uniaxial crystal whose refractive indices of ordinary and extraordinary rays vary with wavelength, there are chromatic variations in the lateral displacement produced by SP and the splitting angle offered by WP. In most cases, it is desired that the lateral displacement and the splitting angle are independent of wavelength, especially for beam-splitting and beam-steering applications. For example, the dispersion in birefringence would lead to image blurring in spectral imager [6] and polarization imager [7–9]. The lateral shear and optical path difference ever were assumed to be a constant to realize interferometry [15, 16]. To get real-time spectral images from massive two-dimensional interference data, sometimes the achromatic optical path difference produced by the SP or WP in birefringent Fourier transform imaging spectrometers are also welcomed [2–5,10–13], instead of accumulating simple or complex rescaling algorithms into the traditional Fourier transformation for the accurate reconstruction of spectral image [1,3, 17–20].

Recently, many efforts were made to overcome the above drawbacks in the aspect of hardware. For instance, achromatic WPs were proposed with the combination of two different crystal materials [21, 22]. This achromatization principle is similar to the design of achromatic wave-plate [23, 24] and doublet lens, and has potential benefits at all wavelengths that achromatic WPs are used, from extreme UV to multispectral and polarization imaging at infrared. Similarly, SP can also be achromatized with the same method, whereas the choices of the materials and thickness ratio are critical. As far as we know, there are no related literatures about the design of achromatic SP so far.

In this paper, the principle for the achromatization of SP is described and several achromatic SPs (ASPs) are formed and simulated. We describe the achromatic model of ASPs in section 2. The simulations for choosing suitable materials and thicknesses to achieve ASPs are implemented in section 3, and the ASPs' performances are demonstrated with ray tracing in section 4. Section 5 is conclusion.

2. Theoretical model

2.1 Simple Savart polariscope

A simple SP and its splitting principle is depicted in Fig. 1. It is a combination of two identical parallel-plane crystal plates. The plates' optic axes make an angle of 45° to their

#202883 - $15.00 USD Received 10 Dec 2013; revised 27 Jan 2014; accepted 15 Feb 2014; published 25 Feb 2014

edge, and their principal sections perpendicular to each other. Referring to literature [25], the *o* and *e* rays emerge from the SP parallel to each other and with a lateral displacement *d* for a given wavelength λ. In the general case, *d* is a somewhat complicated function of the angle between the incident plane and the principal section of the first plate. However, considering the important case in which the incident plane coincides with the principal section, the lateral displacement for oblique incidence is given by the relation [26]:

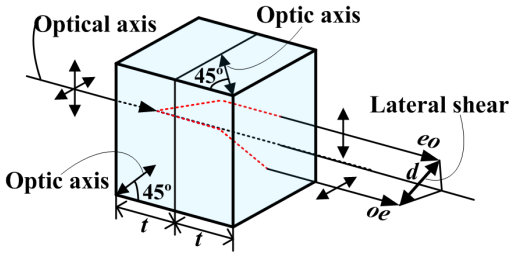

Fig. 1. Optical layout of a simple Savart polariscope.

$$d(t,i,\lambda) = t \cdot B(\lambda) + t \cdot C(\lambda)\sin i + \text{terms in } \sin^3 i, \text{etc.}, \tag{1}$$

where

$$B(\lambda) = \sqrt{2}\,\frac{n_o^2(\lambda) - n_e^2(\lambda)}{n_o^2(\lambda) + n_e^2(\lambda)},\ C(\lambda) = \frac{4n_o(\lambda)n_e(\lambda)}{\left(n_o^2(\lambda) + n_e^2(\lambda)\right)^{3/2}} - \frac{\sqrt{2}}{n_o(\lambda)},$$

i is the angle of incidence, n_o and n_e are the ordinary and extraordinary rays' principal refractive indices of the uniaxial crystal respectively, *t* is the thickness of a single plate. Usually the terms in $\sin^3 i$ is ignored for paraxial approximation. As can be seen, the lateral displacement *d* may be positive or negative which depends on the birefringent sign of material. For the convenience of comparison between the positive and negative crystals, the chromatic variation in the lateral displacement (CVLD) over a spectral range (λ_{min}, λ_{max}) is defined as

$$\Delta d(t,i,\lambda) = \left|d(t,i,\lambda)\right| - \left|d(t,i,\lambda_0)\right|, \tag{2}$$

where $\lambda_0 = (\lambda_{max} + \lambda_{min}) / 2$ is the nominal center wavelength.

2.2 Achromatization of Savart polariscope

According to the splitting principle of the simple SP [26], an ASP can be formed by combining two SPs that are made of two birefringent materials with opposite sign or same sign of birefringence, as illustrated in Fig. 2. For a ray transmitted through the two SPs in sequence, the total lateral displacement are thus expressed as

$$d(t_1,t_2,i,\lambda) = d(t_1,i,\lambda) \pm d(t_2,i,\lambda) = \left(t_1B_1 \pm t_2B_2\right) + \left(t_1C_1 \pm t_2C_2\right)\sin i, \tag{3}$$

where the plus sign means that the two materials have the opposite sign of birefringence, otherwise reverse. Subscripts 1 and 2 denote two different materials. Then the CVLD for the ASP can be written as

$$\Delta d(t_1,t_2,i,\lambda) = \left|d(t_1,t_2,i,\lambda)\right| - \left|d(t_1,t_2,i,\lambda_0)\right|. \tag{4}$$

Achromatization involves a weighted minimization of CVLD across the spectral range λ_{max} to λ_{min} as a function of combinations of thicknesses t_1 and t_2 that yield a nominal lateral displacement $d(t_1, t_2, \lambda_0)$.

#202883 - $15.00 USD Received 10 Dec 2013; revised 27 Jan 2014; accepted 15 Feb 2014; published 25 Feb 2014

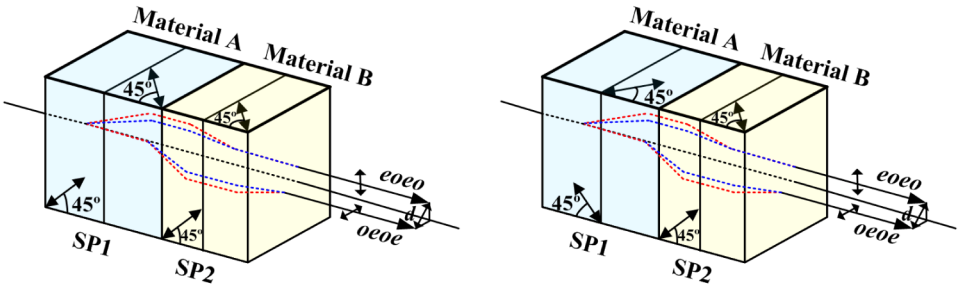

Fig. 2. Illustration of achromatization principle. SP1 and SP2 are made of birefringent materials with (a) the opposite sign and (b) the same sign of birefringence, respectively.

An achromatization around a nominal central wavelength λ_0 can be achieved by taking the derivative of two terms in Eq. (3) with respect to wavelength λ, respectively,

$$\frac{dB_1}{d\lambda}(\lambda_0)t_1 \pm \frac{dB_2}{d\lambda}(\lambda_0)t_2 = 0, \tag{5a}$$

$$\frac{dC_1}{d\lambda}(\lambda_0)t_1 \pm \frac{dC_2}{d\lambda}(\lambda_0)t_2 = 0. \tag{5b}$$

Where plus is for the two materials with opposite sign of birefringence and the crystal axes of the two SPs should be aligned in parallel as shown in Fig. 2(a). Minus is for the two birefringent materials with same sign of birefringence and the crystal axes of the two SPs should be aligned in orthogonal as shown in Fig. 2(b). Correspondingly, two thickness ratios are derived from Eqs. (5):

$$\rho_B(\lambda_0) = \frac{t_1}{t_2} = \mp \frac{\frac{dB_2}{d\lambda}(\lambda_0)}{\frac{dB_1}{d\lambda}(\lambda_0)}, \tag{6a}$$

$$\rho_c(\lambda_0) = \frac{t_1}{t_2} = \mp \frac{\frac{dC_2}{d\lambda}(\lambda_0)}{\frac{dC_1}{d\lambda}(\lambda_0)}, \tag{6b}$$

where the minus sign means that the two materials have the opposite sign of birefringence, otherwise reverse. Generally a pair of t_1 and t_2 cannot satisfy Eqs. (6) simultaneously, therefore the dominate terms in Eqs. (1), (3), and (6) should be determined firstly.

For general materials and an angle of incidence of 10°, the magnitude of the sin$i$ terms in Eqs. (1) and (3) does not exceed 5 percent of the constant terms. Therefore, in most practical cases of interest, the terms in sin$i$ (and thus their achromatic variation) can be neglected in comparison to the constant term, and the thickness ratio in Eq. (6a) should be employed to determine the chromatic compensation of the lateral displacement. Correspondingly, the total lateral displacement and CVLD for the ASP can be approximated as, respectively,

$$d(t_1, t_2, \lambda) = t_1 B_1 \pm t_2 B_2, \tag{7}$$

and

$$\Delta d(t_1, t_2, \lambda) = \left| d(t_1, t_2, \lambda) \right| - \left| d(t_1, t_2, \lambda_0) \right|. \tag{8}$$

#202883 - $15.00 USD Received 10 Dec 2013; revised 27 Jan 2014; accepted 15 Feb 2014; published 25 Feb 2014

3. Simulations and discussions

Based on the above theoretical model, following procedures can be referred to design an ASP. Firstly, choose available materials. Secondly, determinate the thickness ratio at the nominal center wavelength using Eq. (6a) over a considered spectral range. Next, calculate the thicknesses of the two SPs according to the needed lateral displacement at the nominal center wavelength. Finally, assess the ASP's performance across the spectral range by the maximum CVLD, that is the absolute value of the maximum difference between the lateral displacements of any wavelength and that of nominal central wavelength λ_0,

$$\mathrm{Max}\left|\Delta d\right| = \mathrm{Max}\left\|d(t_1,t_2,\lambda)\right| - \left|d(t_1,t_2,\lambda_0)\right\|. \tag{9}$$

Usually, the available materials for the manufacture of SP are YVO_4, $CaCO_3$ (Calcite), α-BaB_2O_4 (α-BBO) and $LiNbO_3$. However, the suitable pairing materials should be determined based on cost, availability, and birefringence. Following dispersion Eqs. (10) are employed for simulations [27], and the unit of wavelength is μm. The spectral range used here is from 0.4 μm to 0.9 μm, then nominal central wavelength is 0.65 μm.

$$YVO_4 \rightarrow \begin{cases} n_o^2 = 3.77834 + 0.069736/(\lambda^2 - 0.04724) - 0.0108133\lambda^2 \\ n_e^2 = 4.59905 + 0.110534/(\lambda^2 - 0.04813) - 0.0122676\lambda^2 \end{cases}, \tag{10a}$$

$$\text{Calcite} \rightarrow \begin{cases} n_o^2 = 2.69705 + 0.0192064/(\lambda^2 - 0.01820) - 0.0151624\lambda^2 \\ n_e^2 = 2.18438 + 0.0087309/(\lambda^2 - 0.01018) - 0.0024411\lambda^2 \end{cases}, \tag{10b}$$

$$\text{α-BBO} \rightarrow \begin{cases} n_o^2 = 2.74710 + 0.01878/(\lambda^2 - 0.01822) - 0.01354\lambda^2 \\ n_e^2 = 2.37530 + 0.01224/(\lambda^2 - 0.01667) - 0.01516\lambda^2 \end{cases}, \tag{10c}$$

$$LiNbO_3 \rightarrow \begin{cases} n_o^2 = 4.90480 + 0.11768/(\lambda^2 - 0.04750) - 0.027169\lambda^2 \\ n_e^2 = 4.58200 + 0.099169/(\lambda^2 - 0.04443) - 0.021950\lambda^2 \end{cases}. \tag{10d}$$

The birefringence $\Delta n = (n_e - n_o)$ of the above materials vary with wavelength is depicted in Fig. 3(a). As can be seen, while YVO_4 is suitable for using to design a thinner SP due to its larger birefringence, α-BBO is suitable for a quasi-achromatic SP attribute to its weaker dispersion. Herein, we assume the needed value of the lateral displacement is $\left|d(\lambda_0)\right| = 1$ mm at the nominal central wavelength λ_0. For the simple SP that is made of a single birefringent material, the CVLD across the spectral range is presented in Fig. 3(b). The needed thickness t of the simple SP, and the maximum CVLD $\mathrm{Max}\left|\Delta d\right|$, are summarized in Table 1. It is found that the simple SP made of α-BBO still has a considerable CVLD of 0.0481 mm.

#202883 - $15.00 USD Received 10 Dec 2013; revised 27 Jan 2014; accepted 15 Feb 2014; published 25 Feb 2014

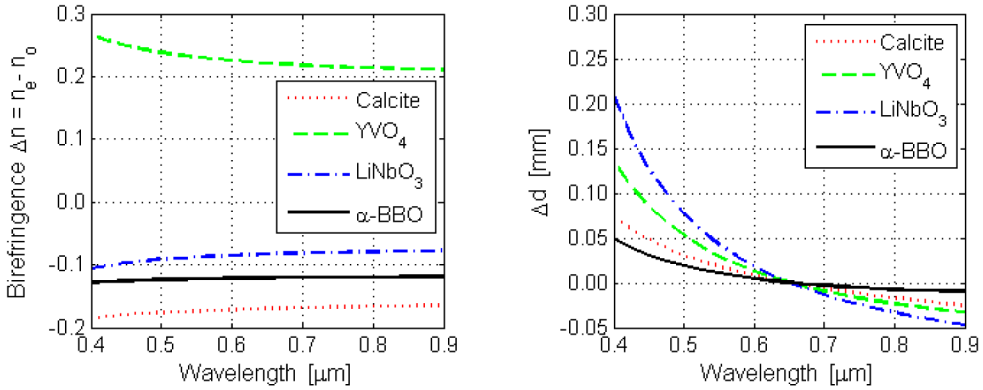

Fig. 3. (a) The chromatic variation in the birefringence of YVO_4, $CaCO_3$, α-BaB_2O_4, and $LiNbO_3$, and (b) the chromatic variation in the lateral displacement (CVLD) for the simple SP that is made of a single birefringent material.

Table 1. Thickness *t* and Maximum CVLD $\mathrm{Max}|\Delta d|$ for the Nominal Lateral Displacement of 1 mm of the Simple SPs that are made from 4 Birefringent Crystals: YVO_4, Calcite, α-BBO, and $LiNbO_3$.

Material	*t* (mm)	*d* (mm)	$\mathrm{Max}\|\Delta d\|$ (mm)
YVO_4	6.55	−1	0.1354
Calcite	6.73	1	0.0735
α-BBO	9.44	1	0.0481
$LiNbO_3$	19.09	1	0.2094

For the ASP that is made from pairing materials, the CVLD across the wavelength range is depicted in Fig. 4. The parameters for six types of ASPs are derived in Table 2. As can be seen, only two pairing materials, α-BBO/YVO_4 and α-BBO/$LiNbO_3$, are suitable for designing ASP when simultaneously consider the advantages of achromatization and size. Coincidentally, the former are two materials with opposite sign of birefringence, and the latter are two birefringent materials with same sign. The reductions in the CVLDs attribute to the above two pairing materials are reduced by about an order of magnitude. The maximum CVLD $\mathrm{Max}|\Delta d|$ of 0.0481 mm for the simple SP that is made of α-BBO is reduced to 0.0025 mm for the ASP that is made of α-BBO/YVO_4. Since the total thickness of the ASP become twice that of the simple SP, the trade-off between the aspect ratio and needed lateral displacement should be considered carefully. According to the state-of-art of the crystal growth technique, it is difficult to grow large YVO_4 currently. Therefore, α-BBO and $LiNbO_3$ are the optimized pairing materials for the achievement of ASP with a larger clear aperture.

#202883 - $15.00 USD Received 10 Dec 2013; revised 27 Jan 2014; accepted 15 Feb 2014; published 25 Feb 2014

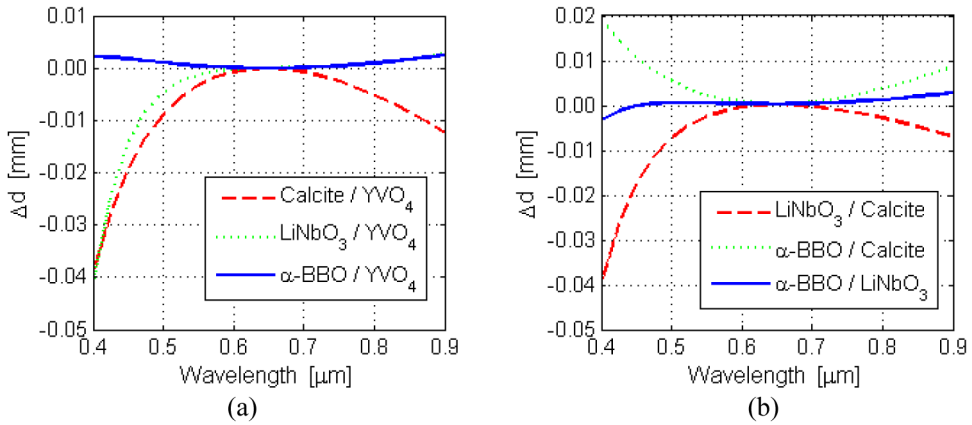

Fig. 4. The spectral variation of the lateral displacement relative to the nominal value for the ASPs that are made of pairing birefringent materials of (a) opposite sign and (b) same sign.

Table 2. Thickness ratio ρ, Individual Thickness t, Individual Lateral Displacement d, and Maximum CVLD $\mathrm{Max}\left|\Delta d\right|$ for the Nominal Lateral Displacement of 1 mm of the ASPs that are Made From Four Birefringent Crystals: YVO_4, Calcite, α-BBO, and $LiNbO_3$.

Pairing Materials	ρ	t_1 / t_2 (mm)	d_1 / d_2 (mm)	$\mathrm{Max}\left\|\Delta d\right\|$ (mm)
Calcite/YVO_4	1.506	18.51/12.29	2.8254/–1.8254	0.0394
$LiNbO_3$/YVO_4	2.000	45.72/22.6	2.3956/–3.3956	0.0415
α-BBO/YVO_4	4.070	14.39/3.54	1.5251/–0.5251	0.0025
α-BBO/$LiNbO_3$	2.035	12.47/6.13	1.3213/0.3213	0.0033
α-BBO/Calcite	2.702	20.21/7.48	2.1423/1.1423	0.0193
$LiNbO_3$/Calcite	1.328	15.99/12.04	0.8377/1.8377	0.0400

4. Ray tracing analysis

As a theoretical demonstration, the above-mentioned parameters of SPs and ASPs are inserted into Zemax software [28] with a 5 mm diameter pupil. Since the dispersion equations of some birefringent materials cited by Zemax software is not consist with Eqs. (10), the modifications of ZEMAX's glass catalogs must be done firstly to match up well with the theoretical calculation.

As discussed above, YVO_4 and α-BBO are two materials that are suitable for the designs of simple SP. After inserting the parameters that strictly copied from Table 1, the on-axis ray tracing configurations of the two simple SPs that made from YVO_4 and α-BBO are shown in Figs. 5(a) and 5(b) respectively. Correspondingly, the on-axis ray shearing diagrams at the last surface of the SPs are shown in Figs. 6(a) and 6(b) respectively. As can be seen, the lateral displacements reduce with the increases of wavelength, that is there are considerable CVLDs in the two simple SPs, although the CVLD of α-BBO is less than that of YVO_4. These phenomena consist with the above theoretical analysis.

#202883 - $15.00 USD Received 10 Dec 2013; revised 27 Jan 2014; accepted 15 Feb 2014; published 25 Feb 2014

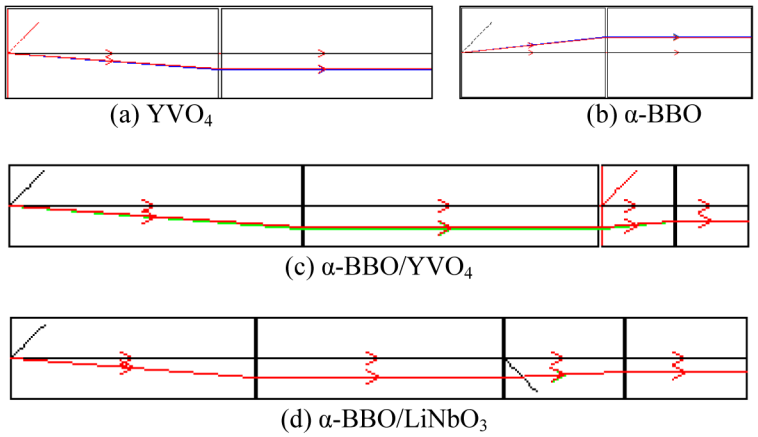

Fig. 5. The on-axis ray tracing configurations of two simple SPs and two ASPs with Zemax software (light passing from left to right).

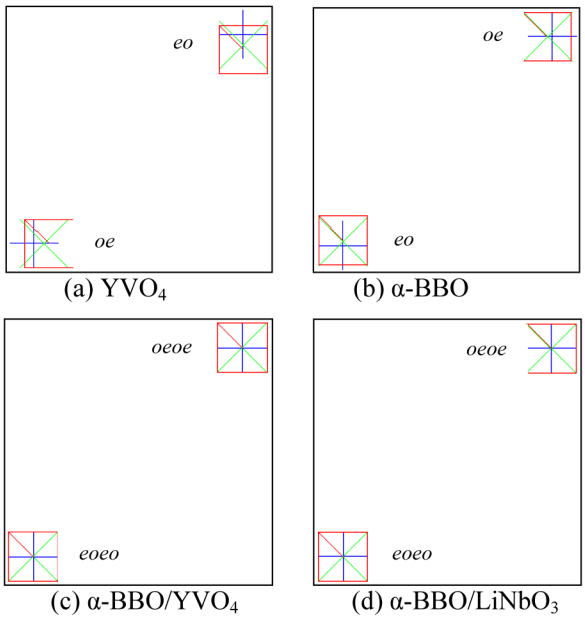

Fig. 6. The on-axis ray shearing diagrams at the last surface of two simple SPs and two ASPs. For visual purposes, one incident ray is shown. The symbols of red rectangle, green reticle and blue cross are used to illustrate the dispersion of different wavelengths.

Similarly, α-BBO/YVO_4 and α-BBO/$LiNbO_3$ are two pairing materials that are suitable for the designs of ASP. After inserting the parameters that strictly copied from Tab. 2, the on-axis ray tracing configurations of two ASPs that made from them are shown in Figs. 5(c) and 5(d) respectively. Figures 6(c) and 6(d) show the corresponding on-axis ray shearing diagrams at the last surface of the ASPs respectively. The CVLDs in the two ASPs almost reduce to zero and the emergent rays of different wavelengths overlap each other, although the thicknesses of the ASPs are considerably larger than that of the simple SPs. As can be seen, the ray tracing software simulation confirmed the developed theoretical model.

However, as described in section 2.1, the determination of the achromatic condition in Eq. (6a) is based on the neglect of the sin$i$ terms in Eqs. (1) and (3). For practical system, especially imaging system, the sin$i$ terms and higher order terms are inevitable. Figure 7

#202883 - $15.00 USD Received 10 Dec 2013; revised 27 Jan 2014; accepted 15 Feb 2014; published 25 Feb 2014

shows the off-axis ray shearing diagrams for the angle of incidence of 10°. As can be seen, the lateral displacements for different wavelengths still approach constant one, there are almost no residual CVLDs. That is the achromatization is also valid for non-normal incidence at paraxial angle. However, the emergent rays of different wavelengths do not overlap each other, and the shorter-wavelength rays shift away from the central-wavelength ray obviously. This issue has no any influence on the fringe pattern formed by the interferometric system that based on the ASPs, such as Fourier transform imaging spectrometry [2,4,5] and spectropolarimetry [11–13] and interferometry [14–16]. However, the issue should be treated carefully in the dual-beam imaging polarimeter [7], because the off-axis object point in the obtained polarization images for different wavelengths will not overlap each other. A band-pass or cut-off filter can be employed to deal with this problem.

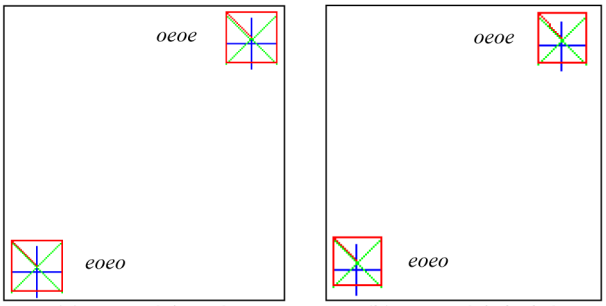

(a) α-BBO/YVO_4 (b) α-BBO/$LiNbO_3$

Fig. 7. The off-axis ray shearing diagrams at the last surface of ASPs. For visual purposes, one incident ray is shown. The symbols of red rectangle, green reticle and blue cross are used to illustrate the dispersion of different wavelengths.

5. Summary

In conclusion, this paper describes the achromatization principle of SP and proposes an effective procedure for the design of ASP. The ASP can be achieved by combining two SPs that are made of two materials with opposite sign or same sign of birefringence. The material selection depends on the advantages of birefringence, achromatization, size, cost, and availability. The theoretical simulation and ray tracing results show that two pairing materials, α-BBO/YVO_4 and α-BBO/$LiNbO_3$, are suitable to the achievement of achromatization among four suggested birefringent materials: YVO_4, Calcite, α-BBO and $LiNbO_3$. The reduction in the chromatic variation of lateral displacement can be reduced by an order of magnitude across the specified spectral range 0.4 μm to 0.9 μm. The thicknesses of the two SPs are determined by the nominal center wavelength of 0.65 μm. The principle of achromatization has potential benefits at all wavelengths where SP may be used, and the price to pay is the increase of size.

Acknowledgments

The authors thank the anonymous reviewers for their helpful comments and constructive suggestions. The work was supported by the Scientific Research Support Program for New Teacher of Xi'an Jiaotong University of China, the Fundamental Research Funds for the Central Universities of China (xjj2013044), the Specialized Research Fund for the Doctoral Program of Higher Education of China (20130201120047), the National Natural Science Foundation of China (61275184), and the National High Technology Research and Development Program of China (2012AA120211).